ACS OMEGA

http://pubs.acs.org/journal/acsodf

Article

Synthesis, Characterization, and Biological Activity of Aminated Zymosan

Geetha Venkatachalam, Senthilkumar Arumugam, and Mukesh Doble*

Cite This: *ACS Omega* 2020, 5, 15973−15982

Read Online

ACCESS | Metrics & More | Article Recommendations | Supporting Information

ABSTRACT: Zymosan (ZM), a naturally occurring insoluble macromolecule obtained from the cell wall of *Saccharomyces cerevisiae*, is used as a functional food (as dietary fiber), phagocytic stimulus, and immune potentiator. The present study aimed to increase its solubility and evaluate its immunological application. ZM was converted into soluble 6-amino-6-deoxy-β-(1-3)-glucan of a molecular weight of 296 kDa by reduction. Detailed structural characterization of aminated ZM was determined by Fourier transform infrared spectroscopy and two-dimensional NMR analysis (2D, COSY, TOCSY, ROSEY, NOSEY, and HSQC). Aminated ZM was biocompatible with Raw 264.7 macrophage cell lines up to a concentration of 100 μg/mL. Rhodamine tagging revealed that the aminated ZM microparticles were found localized within the nucleus of Raw 264.7 cells. Both native and aminated ZM showed a similar expression pattern of inflammatory genes in Raw 264.7.

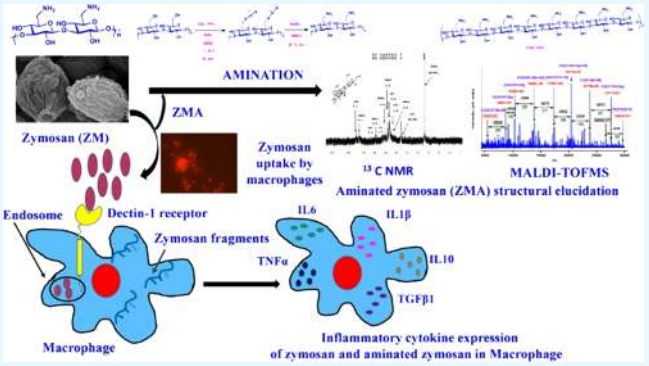

INTRODUCTION

Zymosan (ZM) is an insoluble β-1,3-glucan polysaccharide, extracted from *Saccharomyces cerevisiae,* which plays an important role in the architecture of the host cell wall. Yeast contains β-glucan (1, 3/1, 6-glucan) as the main component along with mannoproteins in the outer layer, nucleic acids[1] and chitin in the inner layer.[2] In general, the immunomodulating activity of different bacterial β-glucans varies depending on the molecular weight, tertiary structure, purity, solubility, degree of branching, conformation in the solution, and charge.[3] They are recognized by the Dectin-1 receptor and complement receptor 3 (CR3) of the immune cells including macrophages, dendritic cells, and neutrophils. They activate both innate and acquired immunity. Direct stimulation of the collagen biosynthesis in fibroblast cells is achieved by β-glucan receptors on human dermal fibroblasts.[4,5]

ZM is an activator of phagocytic cells, which increases the levels of lysosomal enzyme secretion, upregulates the leukotriene production of monocytes, and enhances the release of proinflammatory cytokines, IL6 and TNFα,[6,7] monocyte chemoattractant protein (MCP-1),[8] CXCL1 (Chemokine—C-X-C motif),[9] chemokine IL8,[10] and matrix metalloproteinase 9.[11] Macrophages recognize ZM through the pattern recognition receptors (PRRs) via binding to the pathogen-associated molecular patterns on these polysaccharides[12] including CR3,[13] Dectin-1,[14] lactosylceramide,[15] and scavenger receptors.[16]

Immune-modulatory phytochemicals such as flavonoids, alkaloids, terpenoids, tannins, anthocyanins, glycosides, saponins, polysaccharides, lectins, sterols, and phenolic compounds are naturally occurring and widely used for different disease treatments. Unsaturated fatty acids from seed oil, mushrooms, animals, and plants are used as functional foods for diabetes mellitus and blood sugar control. These liposoluble constituents play a major role in the biomedical field as broad-spectrum therapeutic agents with low toxicity.[17] Dietary flavonoids from fruits, tea, cocoa, and vegetables are bioactive compounds with anti-inflammatory properties. Glycosylation, hydroxylation, and o-methylation are the modification methods for flavonoids with better metabolic features than the parent compounds, which affect the mechanism of inflammation.[18] Polyphenols including flavone, flavonols, flavanone, flavanonol, anthocyanidins, falvan-3-ols, isoflavone, and isoflavanone are found in vegetables, fruits, and beverages. Polyphenols designed as dietary supplements suppress symptoms of disease and improve health.[19] Caffeic acid and chlorogenic acid from *Sonchus oleraceus* Linn crude extract have a synergistic effect and delay hepatic dysfunction and improve hepatic insulin resistance.[20]

Received: March 20, 2020
Accepted: June 11, 2020
Published: June 23, 2020

https://dx.doi.org/10.1021/acsomega.0c01243
ACS Omega 2020, 5, 15973−15982

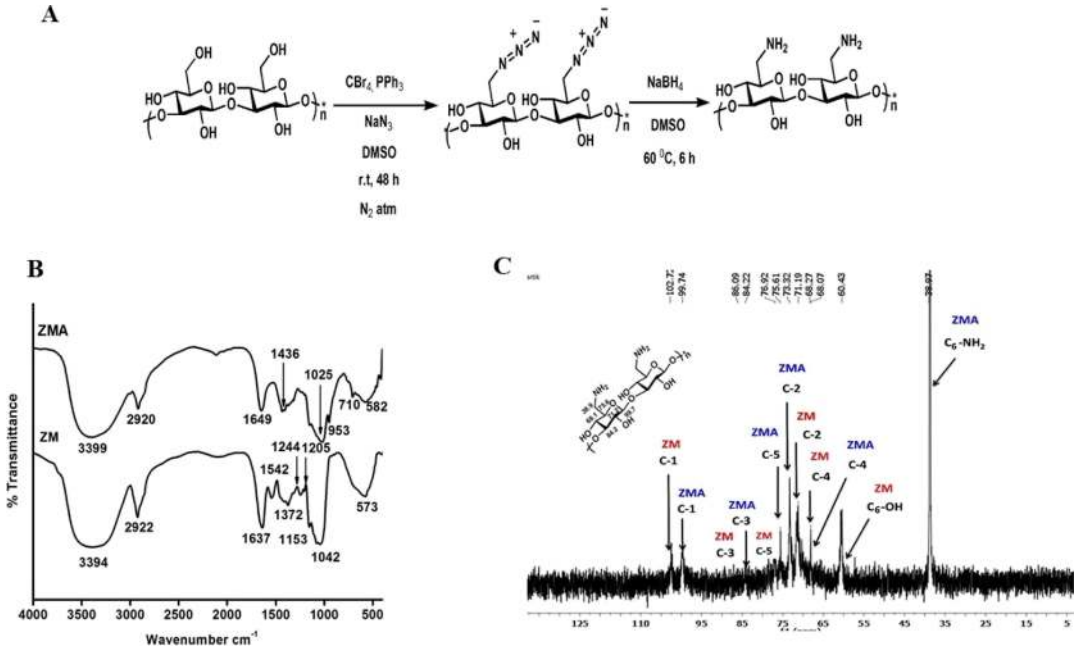

Figure 1. (A) Synthesis scheme for the preparation of ZMA $6NH_2$. (B) FTIR spectrum of ZM and ZMA. (C) ^{13}C NMR spectra of ZMA in D_2O.

ZM has been shown to have the ability to protect and deliver drugs,[21] adjuvants,[22,23] and single-strand DNA[24] and in the adsorption of toxins.[25] ZM has a large and complex molecular structure, and it is insoluble in water (a molecular weight of ~ 296 kDa), which influences its biological effects and absorbance.[22] Several methods have been followed to enhance its bioactivity including hypochlorite oxidation[1] and acid hydrolysis[2,22] to obtain different water-soluble fragments. It has been reported that enhanced water solubility, nucleic acid affinity, and Dectin-1-targeted tissue-specific delivery were achieved with aminated glucans.[26] Partially aminated curdlan retains its original conformation, which facilitates its binding to phagocyte cell surface receptors, and Dectin-1 (PRR). The main objective of this work is to study the immunomodulatory effects (the activation of inflammation-related protein expression) and characterization of ZM and aminated zymosan (ZMA). Reports are there for ZM uses as an immune enhancer. Native ZM is insoluble in water, and it is very difficult to determine its molecular weight and NMR characteristics. Conversion of insoluble ZM to soluble ZM (amination) is the main novelty of this work, which aids in the determination of the ZM high molecular weight (296 kDa) through MALDI-MS-MS. Moreover, the 1D and 2D NMR characterization was achieved after amination. Yeast glucan as food has been used in Japan and Korea for many years. The current work provides some interesting information about ZM which is derived from yeast glucan. Moreover, this is a basic study, and a detailed study on its applications will be done in the near future. The present study aimed to synthesize water-soluble ZM without modifying its basic structure through amination and to predict the structure of ZMA.

RESULTS AND DISCUSSION

Amination of ZM. The first step in amination is to chemically modify ZM by replacing the hydroxyl group (−OH) in the C_6 position of the glucose residues with an amino group ($-NH_2$) (Figure 1).[26,27] Under controlled conditions, ZMA was synthesized with 6-azido substitution. This was further reduced into C_6 amine-functionalized ZMA (80% amine substitution). At the end of amination, a biocompatible amine-bearing ZM was synthesized. In the previously reported methods, synthesis of acid/alkali or heat treated ZM, the polymer lost its core activity in the immune system because it was degraded into different fragments and lost active functional groups during the process.[1,28]

FTIR Analysis of ZM and ZMA. Two intense broad bands at 3394 and 3399 cm^{-1} indicated the O−H stretch of the hydroxyl groups in ZM or the N−H stretch in ZMA (Figure 1B). Bands at 2922 and 1244 cm^{-1} indicated the C−H stretch and CH_2OH stretch, respectively. The band at 1372 cm^{-1} could be attributed to the C−H band, and the band at 1637 and 1649 cm^{-1} could be attributed to the C═O group or N−H bend in ZM and ZMA, respectively. The band at 1042 and 1025 cm^{-1} could be attributed to the C−O−C or C−N stretch. ZMA exhibits a new absorption band at 1436 cm^{-1}, which is the characteristic peak of the NH amine. Beta glycosidic linkage was analyzed through Fourier transform (FT)-Raman spectroscopy (Figure S1) at 896 and 891 cm^{-1} for ZM and ZMA, respectively. Moreover, the bands at 953−710 cm^{-1} could be attributed to NH wagging with respect to previous reports on aminated oat beta glucan[29] and aminated chitosan.[30] These results clearly indicated the distribution and the presence of amino groups in ZMA. There was no clear NH_2 peak in the ZMA spectrum which could be attributed to its overlapping with the hydroxyl group peak.

Structural Characterization of ZMA—2D NMR. NMR spectral data revealed the information of the repeating sugar units, configurations, linkages, chain length, and substitutions in the side chain of the polysaccharide.[31,32] In ZMA, the hydroxyl group (^1H NMR, Figure S2) at the C_6 position of the glucose unit was replaced with an amine similar to previous reports.[27] The degree of polymerization (DP) of 6-amino-ZM was determined by ^{13}C NMR (Figure 1C). The C_6−OH of the unmodified glucose unit of ZM appeared at ^{13}C δ 60.4 (C-6); ^1H δ 3.81 (2H, $6H_a$, H_b); after amination, the C_6 shifted to ^{13}C δ 38.97 ppm; ^1H NMR δ 2.61 (2H, $6H_a$, H_b). ZMA shows a

https://dx.doi.org/10.1021/acsomega.0c01243
ACS Omega 2020, 5, 15973−15982

C_6-OH: C_6-NH_2 ratio of 2:8, which is used for determination of the degree of substitution (DS). In the case of 6AZ-80 (80% amine substitution), the ratio of C_6-OH: C_6-NH_2 intensity was about 2:8. ^{13}C NMR analysis of C_6 glucose units revealed the signal at δ_c 60.4 (C-6) in unmodified ZM shifted to δ_c 38.9 (C-6) in 6AZ-80, which indicates that 6-amino ZMA was successfully synthesized, as shown in Figure 1.

The structure of ZMA was elucidated by ^1H, ^{13}C, and 2D ($^1H-^1H$, TOCSY, $^1H-^{13}C$, HSQC, $^1H-^1H$ NOESY, and $^1H-^1H$ ROSEY) NMR spectral analysis. The above analysis was used to assign the proton and carbon signals of the ZMA backbone. The presence of the anomeric proton (δ_H 5.32, 1H), sugar protons (δ_H 3.43−3.70, H2, H3, H4, H5, H6a, H6b, 6H), and the higher field signal (δ_H, 5.32, 1H) in the ^1H NMR spectrum revealed the β-configuration of glucose in the ZMA structure. The ^1H and ^{13}C NMR chemical shift data analysis from different NMR spectra of ZMA and ZM was tabulated (Table 1).

Table 1. ^1H NMR and^{13} C NMR Chemical Shifts of ZM and ZMA (^1H NMR 500 MHz, ^{13}C NMR 125 MHz, D_2O)

position	ZM literature (δ_c)	ZMA 6-NH_2 (δ_c)	ZMA 6-NH_2 (δ_H)
C-1	103.01	99.74	5.32
C-2	72.83	71.19	3.55
C-3	86.22	84.22	3.70
C-4	68.41	68.07	3.43
C-5	76.33	75.61	3.48
C-6	60.87	38.97	2.64

The HSQC spectrum of 6AZ-80 (Figure 2A) provides the information on correlation between ring ^1H and ^{13}C. The ^{13}C chemical shifts of the 6-AZ-80 residue was obtained based on the $^{13}C-^1H$ cross peaks at δ_c/δ_H 99.74/5.32 (C-1/H-1), 71.19 ppm/3.55 ppm (C-2/H-2), 84.22 ppm/3.70 ppm (C-3/H-3), 68.07 ppm/3.43 ppm (C-4/H-4),75.61 ppm/3.48 ppm (C-5/H-5), 38.97 ppm/2.61 ppm (C-6/Ha-6), and 38.97 ppm (2.64 C-6/Hb-6) in the HSQC spectrum. Based on the HSQC spectrum which gives connectivity of protons, their chemical shifts at δ_H 5.32, 3.55, 3.70, 3.43, 3.48, 2.61, and 2.64 were assigned to H-1 and H-2, H-3, H-4, H-5, H-6a, and H-6, respectively, and enhanced the elucidation of the proton peak of ZMA. Similarly, ZMA showed six major peaks at chemical shifts of δ_c 102.72, 73.32, 86.09, 68.27, 76.92, and 60.43 ppm, and these were assigned to C-1, C-2, C-3, C-4, C-5,C-6, respectively, and could be assigned to the signals of the backbone chain for a β-(1,3) ZMA. The chemical shifts of the protons and carbons were obtained from the $^1H-^{13}C$ HSQC, $^1H-^1H$ NOSEY, and H^1-H^1 TOCSY with ^1H and ^{13}C resonances assigned in Table 2. The chemical shift data revealed from the ^{13}C NMR and $^1H-^{13}C$ HSQC spectra of the current work were consistent with those revealed from the spectrum of the curdlan-type polysaccharide.[33] $^1H-^1H$ COSY and $^1H-^{13}C$ HSQC 2D correlation NMR experiments were used to the peak assignment of ^1H, ^{13}C and elucidate the exact β-linkages of the sugar residues within the polysaccharide.[34] Based on HSQC spectra, single-bond correlation studies between the protons and carbons from sugars in ZMA enabled all the ^{13}C to be assigned.[31,35]

The ^1H chemical shift data values obtained from the HSQC spectrum were then verified by the cross peaks of H-1/H-2 (5.31 ppm/3.54 ppm), H-1/H-3 (5.32 ppm/3.66 ppm), and H-1/H-6 (5.32 ppm/3.86 ppm) in the TOCSY spectrum (Figure 2B). The cross peak of H-1/H-3 (5.32 ppm/3.74 ppm), H-1/H-5 (5.32 ppm/3.48 ppm) was also observed in the NOESY spectrum (Figure 2C).

The anomeric resonances for the H-1 proton signal were found in the high field region (H > δ 5.0), and the anomeric resonance for the carbon C-1 signal at δ 99.74 was in the deshielded region along with the scalar coupling constant $^3J_{H\text{-}1\text{-}H\text{-}2}$, which gives the information about the anomeric configuration, and this value was found at 7.0 Hz. These results confirm that ZMA had sugar units of the β-configuration form. Large coupling constants of $J_{H\text{-}2,\ H\text{-}3}$ and $J_{H\text{-}3,\ H\text{-}4}$ (9−10 Hz) indicated that the glucose units were linked with β-glycosidic bands.[26] A NOESY experiment revealed inter-residue NOE connectivity in ZMA, which was observed between H-1, H-3, and H-5, indicating that the residue was a β-configuration. Similarly, a ROSEY (Figure 2D) experiment revealed inter-residue connectivity that was observed between H-1, H-2, and H-6 and H1−H2, H2−H3, H3−H4, H2−H6, indicating that the residue was linked by the β-configuration.

The ^1H,^{13}C NMR spectrum and 2D $^1H-^1H$ COSY, $^1H-^1H$ TOCSY, $^1H-^{13}C$ HSQC, $^1H-^1H$ NOESY, and $^1H-^1H$ ROSEY results confirm that glucose was the main unit in the ZMA polymer with a molecular weight of 2.04753×10^5 Da with β-(1,3) linkage as the main backbone. Such a conformation was repeated in the intercellular matrix of the cell wall of most fungi and yeasts.

MALDI-TOF-MS Analysis of ZMA. The presence of the glucose monomer in ZMA was observed in MALDI-TOF-MS as sodiated and protonated ions $[M + Na + H]^+$ in the positive ion mode. The singly charged molecular ion mass was calculated as $[162 \times n + 3Na + 9H]^+$, where n represents the number of glucose units. The mass region of ion peaks was observed, and the peak-to-peak difference was $162.3 \times n$ Da, which was consistent with the repeating units of ZMA.

The MALDI-TOF mass spectrum (Figure 3) showed the most intense peak at 204,759.200 Da $[162 \times 1264 + 3Na + 9H]^+$ with the second most intense peak at 14,769.29 $[162 \times 91 + H_2O + 5H]$. The peaks at an m/z of 10,068.50 $[162 \times 62 + Na]^+$, 11,862.82 $[162 \times 73 + 2H_2O]^+$, 13,304.15 $[162 \times 82 + H_2O]^+$, 13,743.46 $[162 \times 87 + 5H]^+$, 14,099.40 $[162 \times 82 + H_2O]$, 53,003.052 $[162 \times 327 + Na + 6H]^+$, 86,832.052 $[162 \times 536 + 3Na]^+$, 102,997.620 $[162 \times 636 + 2Na]^+$, 138,562.294 $[162 \times 855 + 2Na + 6H]^+$, 173,837.360 $[162 \times 1073 + 11\ H]^+$, 204,759.200 $[162 \times 1264 + 3Na + 9H]^+$, 237,798.636 $[162 \times 1468 + 9H]^+$, 237,798.636 $[162 \times 1468 + 9H]^+$, 276,110.633 $[162 \times 1704 + 3Na]^+$, and 296,945.816 $[162 \times 1833 + H]^+$ were observed in ZMA.

Based on the MALDI-TOF mass analysis, the molecular weight and the sugar sequences were determined. The spectra showed highly branching units of glucose residues and the most intense peak at an m/z of 204,759.200, which represents the major component with a DP size of 1264 glucose residues. The DP varies from 62 to 1833. This is the first report on MALDI-TOF MS analysis for a very high molecular weight glucan.

ZM is a highly branched, insoluble polymer, whereas the aminated form not only aids in solubilizing but also helps to elucidate its structure without modifying the internal structure. Although high-molecular-weight polymers such as galactomannans (100×10^4 Da) and baker's yeast beta-glucans[2] have been structurally characterized, the exact molecular weight was not estimated because of their size and insolubility. There are many reports on low-molecular-weight glucans from *Rhi-*

https://dx.doi.org/10.1021/acsomega.0c01243
ACS Omega 2020, 5, 15973−15982

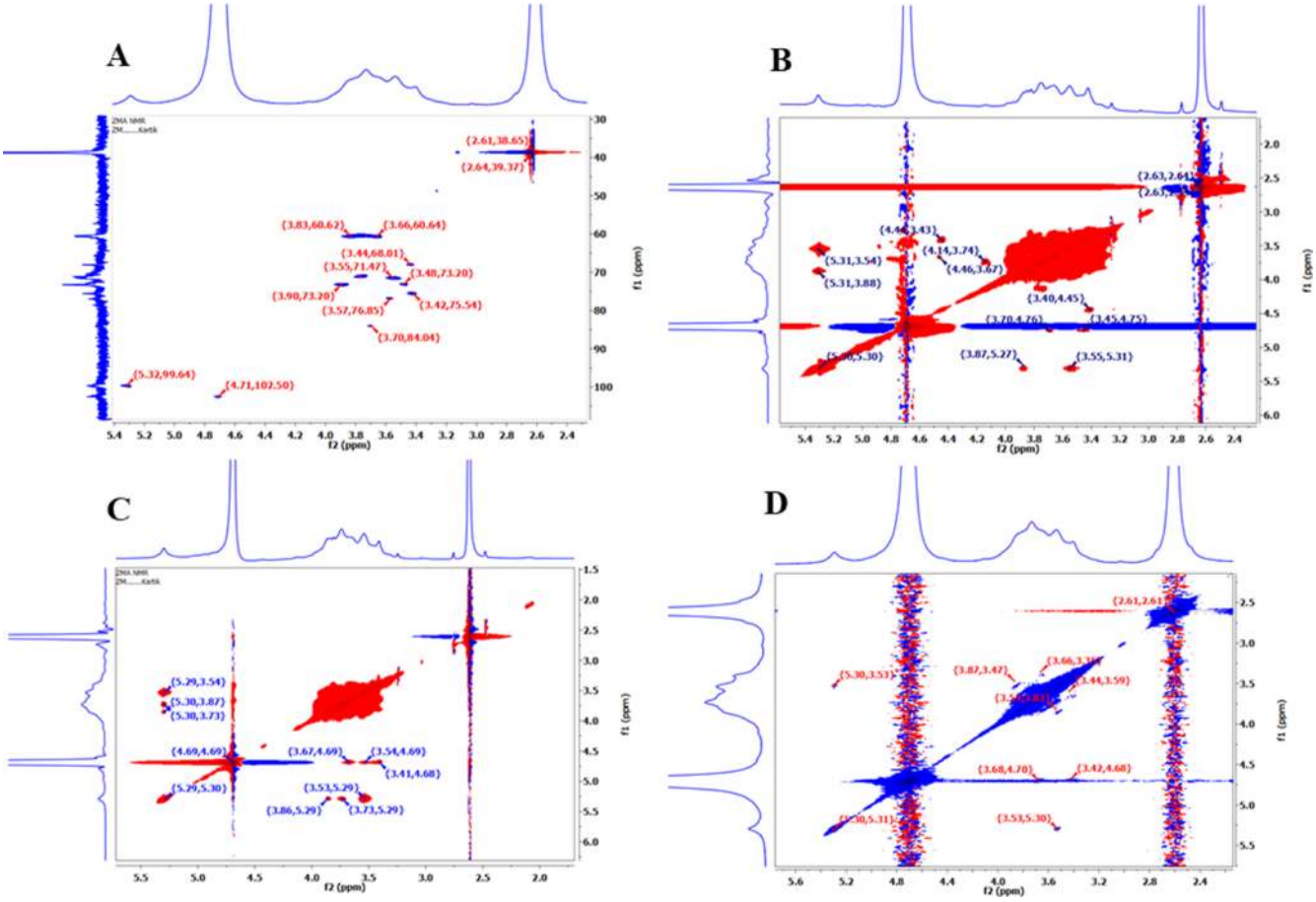

Figure 2. 2D NMR (500 MHz) spectra of ZMA, (A) $^{1}H-^{13}C$ HSQC, (B) $^{1}H-^{1}H$ TOCSY, (C) $^{1}H-^{1}H$ NOESY, and (D) $^{1}H-^{1}H$ ROESY.

Table 2. HSQC, NOSEY, and TOCSY Correlation Map of ZM and ZMA (500 MHz in D_2O)

	HSQC ^{1}H and ^{13}C correlation (ppm)		NOSEY	NOSEY	TOCSY	TOCSY
position	ZM-20 6-OH δ_c/δ_H	ZMA-80 6-NH_2 δ_c/δ_H	ZM-20 6-OH δ_H/δ_H	ZMA-80 6-NH_2 δ_H/δ_H	ZM-20 6-OH δ_H/δ_H	ZMA-80 6-NH_2 δ_H/δ_H
C-1	102.72/4.69	99.74/5.32	4.69	5.32	4.69	5.32
C-2	73.32/3.47	71.19/3.55			3.45	3.54
C-3	86.09/3.60	84.22/3.70	3.60	3.74	3.60	3.66
C-4	68.27/3.34	68.07/3.43			3.27	
C-5	76.92/3.57	75.61/3.48	3.57	3.48		
C-6	60.43/3.81/3.75	38.97/2.64				3.86

zobium meliloti[36,37] and *Mesorhizobium loti*[38] but not on highly branched ones. Molecular weight determination of ZM through acid and/or alkali treatments[39] yielded three different fragments of sizes of 8, 5, and 2 kDa,[22] but till date, there is no experimental report on its solubility.

Microscopic and Particle Size Analysis. ZM appeared as an oval-shaped particle with a size below 3 μm (Figure 4A), whereas ZMA appeared oval, but the morphology was not well-defined (Figure 4B). The particle size distribution of ZM (1−3 μm; Figure 4C) was marginally larger than that of ZMA (< 2 μm; Figure 4D). It was reported that the size of β-glucan particles does not affect its cellular uptake by macrophages, and microparticles of a size of 1−5 μm are readily phagocytosed by macrophages through the Dectin-1 receptor.[40] The hollow and porous structures of yeast beta-glucans (2−4 μm in diameter) were used as microcarriers, and because the porous channels in the glucan shell were not uniform in size, they could help in loading drug molecules with different size distributions.[41] In water suspension, the average size of ZM (Figure S3A) particles was 712.5 ± 7.9 nm with a zeta potential of 9.76 mV, while the average size of ZMA (Figure S3B) particles was 650.0 ± 38.93 nm with a zeta potential of 25.22 mV. The higher zeta potential values indicated the stability of ZMA particles. In general, particles within the size range of 1−1000 nm could be used for prophylactic vaccine designing, with ZM reported as an immunepotentiator; it makes ZMA an ideal carrier molecule for vaccine delivery.

AFM Visualization of ZM and ZMA. The height and amplitude of the scanning field in atomic force microscopy (AFM) revealed a scattered distribution of particles. When compared to ZM (a width of 1.345 μm and a height of around 0.628 μm, as shown in Figure S4A,B), ZMA (Figure S4C,D) was slightly less in size (a width of 1.077 μm and a height of 0.541 μm), which is in line with SEM and particle size analysis, which could be attributed to the solubility. Similar size ranges

https://dx.doi.org/10.1021/acsomega.0c01243
ACS Omega 2020, 5, 15973−15982

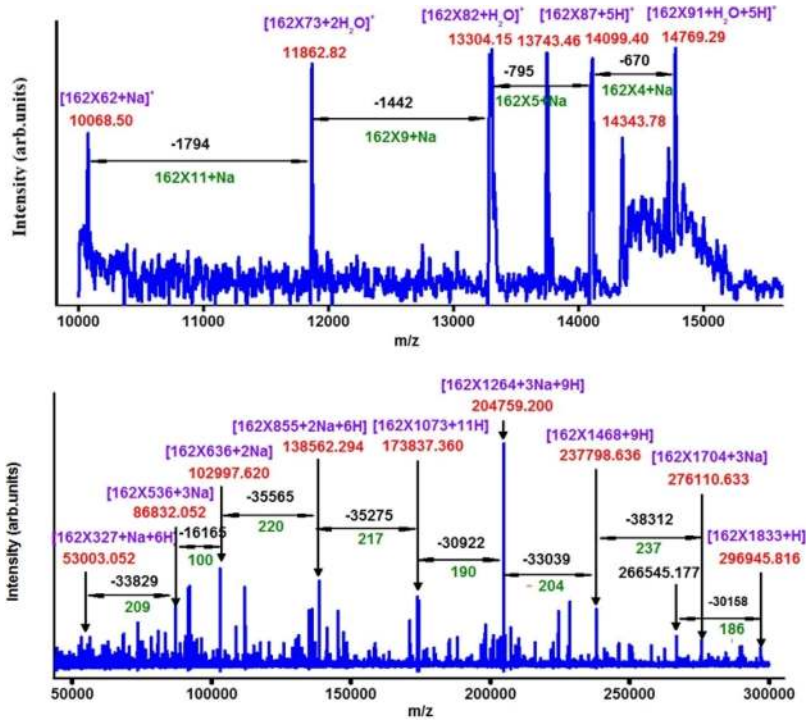

Figure 3. MALDI-TOF mass spectrum of ZMA using CHCA as the matrix. A mass difference of 162.1 Da was observed between neighboring peaks. The ions were singly charged $[M + Na]^+$ and observed in the positive ion mode and are consistent with the expected mass.

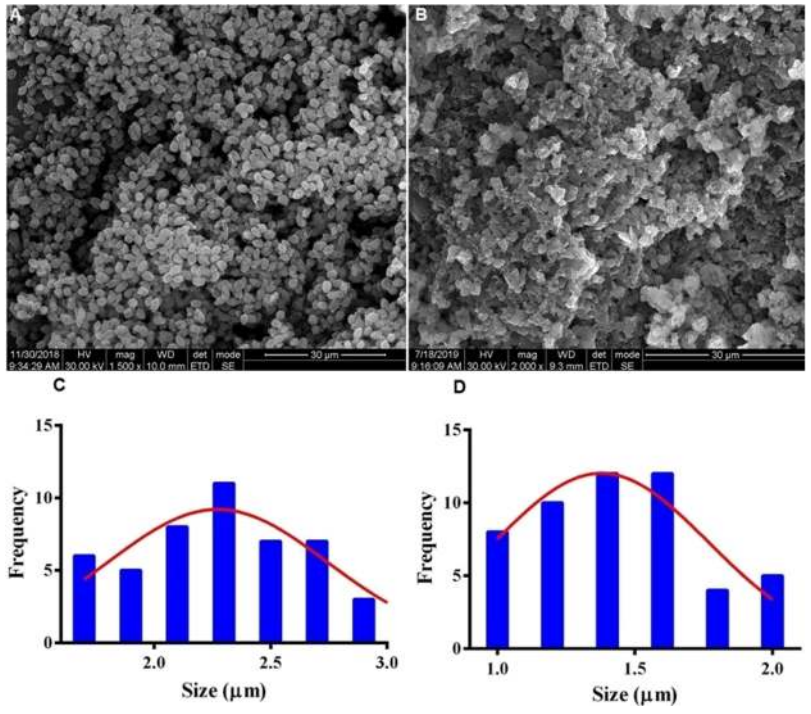

Figure 4. SEM images of (A) ZM and (B) ZMA microparticles. Size distributions of (C) ZM and (D) ZMA microparticles.

have also been reported with yeast β-glucan films (2.70 μm) and particles (1−2 μm).[42,43]

ZM and ZMA Biological Activities in Mouse Raw 264.7 Cell Lines. Raw 264.7 macrophage cells are majorly involved in the phagocytic process. They have the Dectin 1 receptor on their surface, which recognizes beta (1,3)-glucans. Our aim is to study the immunomodulatory effects of beta (1,3)-glucan on macrophage cells, so the Raw 264.7 cell line was chosen for this study. ZM has the ability to bind to the Dectin-1 receptor present on macrophages. Therefore, cell viability, cell uptake, and gene expression analysis were carried out in mouse Raw 264.7 cells.

Cell Viability. Both ZM and ZMA (Figure S5) were not cytotoxic to Raw 264.7 cells, and the cell viability was above 90%, which could be considered nontoxic according to ISO

https://dx.doi.org/10.1021/acsomega.0c01243
ACS Omega 2020, 5, 15973−15982

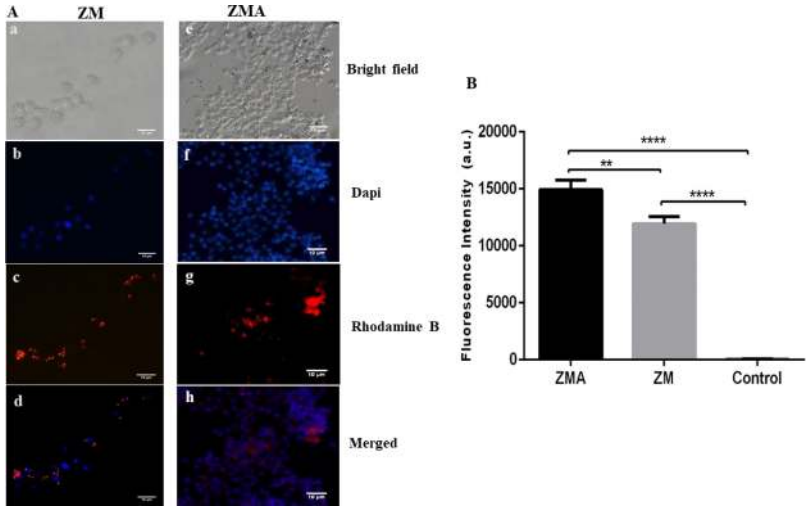

Figure 5. (A) Fluorescence microscopy images of Raw 264.7 macrophages. Rhodamine B-tagged ZM particles (a–d) and ZMA particles (e–h). (B) Quantified fluorescence intensities (**P < 0.01, ****P < 0.0001).

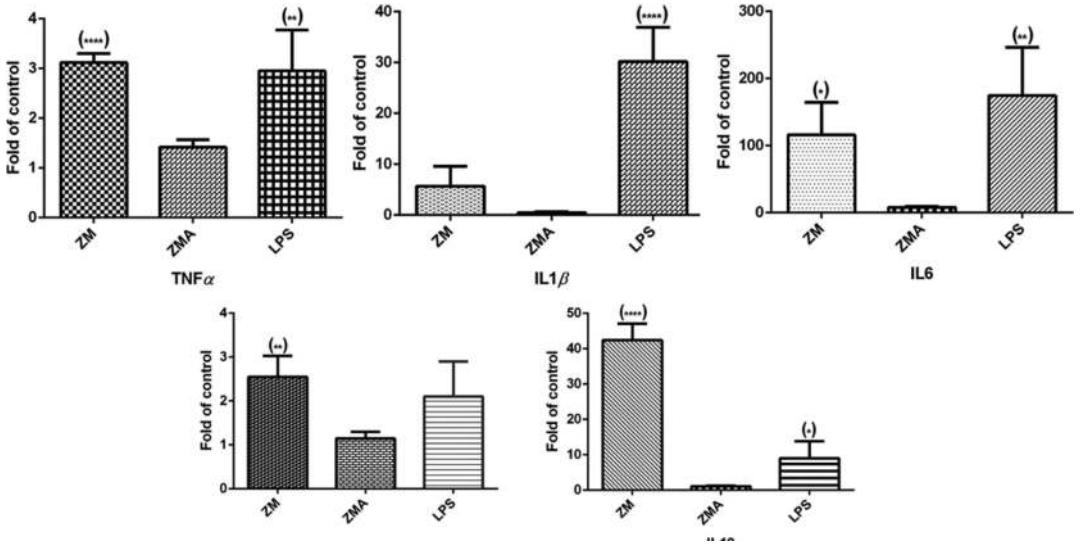

Figure 6. Expression of inflammatory cytokines in macrophage cells with ZMA and LPS treatment. *p < 0.05, **p < 0.001, and ****p < 0.0001 are with respect to the control (cells without the polymer and LPS treatment).

10993-5.[44] This is in line with other biocompatibility studies reported with other bacterial glucans[37,45,46] and yeasts.[47]

Cell Uptake. ZM and ZMA were observed as red particles inside the cell. Both ZM (Figure 5a–d) and ZMA (Figure 5e–h) showed a similar pattern of uptake. Phagocytic and dendritic cells are potentially important targets in RNAi-based therapeutics, and ZM has been reported as a host for siRNA and drug delivery.[24,48] ZM has the ability to bind to the Dectin-1 receptor of the macrophages, which stimulates the inflammatory response by chemokine and cytokine production (innate immune responses) as well as the antimicrobial effect through phagocytosis and generation of reactive oxygen species which further influences the adaptive immunity.[49,50]

Increased intracellular fluorescence in Raw 264.7 macrophages (Figure 5B) with both ZM and ZMA could be attributed to the receptor-mediated phagocytosis and passive uptake through steric or van der Waals interactions.[51] Studies have indicated that sharp-edge particles showed less internalization than spherical particles. This could be attributed to the less energetic cost of initializing membrane curvature during phagocytosis of spherical particles.[52]

ZMA was biocompatible with Raw 264.7 cells, and the cellular uptake was similar to ZM. These studies indicate that ZMA has potential applications in medical imaging and drug delivery systems.

Gene Expression of ZM and ZMA in Raw 264.7. Levels of inflammatory (TNFα, IL1β, and IL6, TGFβ1, and IL10)[46] in Raw 264.7 with ZM, LPS, and ZMA were analyzed using real-time PCR analysis (Figure 6). Increased expression of both pro- and anti-inflammatory cytokines was observed in all three treatments. The fold change for TNFα, IL1β, and IL6 with respect to LPS treatment was 2.95, 30.20, and 174.29, respectively, whereas with ZM, it was TNFα (3.18), IL1β (5.66), and IL6 (115.76), and with ZMA, it was TNFα (1.42-fold), IL6 (7.77-fold), and IL1β (0.47-fold). The fold increase of the anti-inflammatory cytokines with respect to the treatments was TGFβ1 (2.54) and IL10 (42.38) with ZM, TGFβ1 (2.10) and IL10 (9.04) with LPS, and TGFβ1 (1.14) and IL10 (1.10) with ZMA.

https://dx.doi.org/10.1021/acsomega.0c01243
ACS Omega 2020, 5, 15973–15982

Amination of ZM showed a statistically significant difference in the regulation of IL6. Although ZM binds to the Dectin-1 receptor present in the macrophage, it is widely used as a phagocytic stimulus.[53,54] The two-step amination process solubilized ZM, and there was no significant difference in cell viability or cellular uptake. TLR activation of microglia cells (active immune cells of the central nervous system) by ZM led to upregulation of proinflammatory genes, TNF-α, IL-6, and IL-1β, which are also resident macrophage cells.[54]

CONCLUSIONS

This is the first approach to increase the solubility of ZM by partial amination without affecting its native structure. The compound 6-azido-6-deoxy-ZM was synthesized and reduced further to 6-amino-6-deoxy-ZM. ZMA is highly branched with the DP ranging from 62 to 1833 glucose residues with increased solubility and a reduced particle size (1−2 μm). ZMA was biocompatible, and the cellular uptake was similar to ZM with decreased inflammatory effects compared to ZM. ZMA could be a potential candidate for immune modulation and drug delivery.

EXPERIMENTAL SECTION

General Procedure. ZM (#Z4250-1G) was obtained from Sigma Aldrich. The D_2O solvent (deuteration degree, minimum 99.96%) and Methanol D were obtained from Merck. Dialysis membrane-150 (Himedia MW cutoff: 12 kDa), DMSO (dimethyl sulfoxide), $NaBH_4$ (sodium borohydride), methanol, and other chemicals were purchased from Himedia Laboratories Pvt. Ltd.

6-Azido-6-deoxy-(1-3)-β-D-zymosan Synthesis. Amination was carried out, as shown in Figure 1A. ZM (1.0 g) was taken in a two-necked round-bottom flask, and NaN_3 (4.0 g, 61.52 Mmole) was added, dissolved in DMF (dimethylformamide) (30 mL), and stirred well for 30 min. The reaction flask was kept at 80 °C under a nitrogen atmosphere for 2 h. The reaction mixture was cooled to room temperature, and Ph_3P (triphenylphosphine) (4.0 g, 15 Mmole) was added and stirred well. In an inert nitrogen atmosphere, freshly prepared CBr_4 (carbon tetrabromide or tetrabromomethane) (5.5 g, 16 Mmole) solution was added in drops and incubated for 48 h at room temperature.[27] Acetone was used to precipitate the azide and washed thrice with methanol, followed by water. The polymer was freeze-dried and stored.

6-Amino-6-deoxy-(1-3)-β-D-zymosan Synthesis by the Reduction Method. 6-Azide (0.5 g) was dissolved in 30 mL of DMSO and stirred for 30 min at room temperature. $NaBH_4$ (1.2 g, 31 Mmole) was added, and the mixture was heated to 60 °C.[55] The reaction mixture was maintained under continuous heating and stirring (6 h). Later, the aminated glucan was cooled at room temperature and centrifuged at 13,000 rpm. The precipitate was washed thrice with methanol, followed by dialysis using a 12 KDa membrane and then freeze-drying (a yield of 0.45 g).

Characterization of ZMA. The presence of characteristic amino and other functional groups in ZMA was confirmed by Fourier-transform infrared spectroscopy with the attenuated total reflection mode (Perkin Elmer System, Country). FT-Raman spectroscopy (50−5000 cm^{-1}) was carried out for the β-glycosidic linkage analysis using a BRUKER RFS 27 standalone FT-Raman spectrometer. 1 D ^1H NMR (500 MHz), ^{13}C NMR (125 MHz), and 2D NMR with heteronuclear single-quantum coherence (HSQC), H−H correlation spectrometry (COSY), TOCSY, and ROSEY spectra analysis were carried out with a Bruker Avance III 500 NMR (500 MHz). Spectral measurements were carried out at 37 °C and analyzed using the Bruker top spin 3.2 software. D_2O (deuteration degree, minimum 99.96%) and Methanol D were used as NMR solvents.

Determination of the Molecular Weight by MALDI-TOF Analysis. Molecular weights of ZMA were recorded with a Bruker Ultraflex III MALDI-TOF mass spectrometer (with 40,000 mass resolving power with 1 ppm mass accuracy). Acetonitrile (90% v/v) and saturated acyano-4-hydroxycinnamic acid (10% v/v) in TA90 (90% acetonitrile and 0.01% trifluoroacetic acid) were used to run ZMA in the matrix. ZMA was ionized in the positive ion mode, and the spectrum was obtained in the reflector mode, with a laser intensity between 20 and 25%, by accumulating 1000 shots with 0−4000 Da as the detection range. The background noise was eliminated by suppressing the mass signals ($<m/z$ = 200).

SEM and Particle Size Analysis. The prepared polysaccharide particles were detected using a scanning electron microscope (FEI Quanta FEG 200-High Resolution).[56] One milligram of ZM and ZMA was suspended in 1.0 mL of distilled water and vortexed to make a homogeneous suspension, and the corresponding size distribution of the particles in each sample was analyzed using a Zetatrac-Zeta potential particle size analyzer (Microtrac Inc.).[57]

Atomic Force Microscopy. The sample solution (10 μL, 100 mg/mL) was added onto the surface of a clean glass slide and left overnight for the particles to adhere at room temperature. The surface of the glass slide was analyzed using a Park systems X-100 atomic force microscope at room temperature under the noncontact mode to determine the microstructures. All images were taken with a resolution of 512 × 512 pixels on the 20 × 20 μm scale for ZM and 10 × 10 μm scale for ZMA.[58]

Cell Viability of ZM and ZMA. The biocompatibility of ZM and ZMA toward Raw 264.7 cells was analyzed by the (3-(4,5-dimethylthiazol-2-yl)-2,5-diphenyltetrazolium bromide) MTT assay.[59] Raw 264.7 cells (10^4 cells mL^{-1}) were cultured with DMEM for 24 h. Different concentrations of ZM and ZMA (100, 80, 60, 50, 40, 30, 20, and 10 μg mL^{-1}) were added to the cells and incubated in a 5% CO_2 incubator for 24 h. MTT (5 mg mL^{-1}) was added and incubated for 4 h. DMSO was used to solubilize the formazan crystals formed, and the absorbance was measured at 690 and 570 nm using an Enspire Perkin Elmer multimode plate reader (Singapore).

Raw 264.7 Macrophage Cellular Uptake. Rhodamine B- tagged ZM and ZMA samples were synthesized by mixing 1 mg of polymer samples with the fluorescent dye Rhodamine B (100 μg/mL) vortexed and incubated in the dark at 37 °C for 24 h.[45] The particles were centrifuged at 13,000 rpm and washed thrice with phosphate-buffered saline to remove the excess dye and lyophilized (at a temperature of −80 °C). Raw 264.7 cells (1×10^5 cells/mL) were incubated with rhodamine B- tagged particles for 3 h in a CO_2 incubator. The cells were washed several times with PBS. Paraformaldehyde (4%) was used for fixing the cells (20 min at 37 °C) and visualized under an Olympus BX51 fluorescence microscope (Olympus America Inc., USA).

Similarly, Raw 264.7 cells treated with Rhodamine B-tagged ZM and ZMA particles were lysed using a lysis buffer and centrifuged at 13,000 rpm, and the fluorescence was measured

https://dx.doi.org/10.1021/acsomega.0c01243
ACS Omega 2020, 5, 15973−15982

at an excitation of 540 nm and an emission of 575 nm using an EnSpire microplate reader, Perkin Elmer, Singapore.

Inflammatory Gene Expression. Raw 264.7 (1×10^5 cells/mL) cells were cultured in a six-well plate for 24 h, and the medium was replaced with ZM or ZMA (0.5 mg/mL in DMEM). Lipopolysaccharide (10 μg mL^{-1}) was the positive control to induce an inflammatory response. Cells without LPS were used as the control.[60] After 6 h of incubation, the cells were washed twice with PBS, and total RNA was isolated using an RNAiso Plus (Total RNA extraction reagent, Takara Bio Inc., Japan) by following the manufacturer's protocol. Reverse transcription was carried out for 1 μg of RNA with a cDNA Reverse Transcription Kit (Applied biosystems, Thermo Fischer Scientific, USA). The primer sequences of inflammatory genes used in this current work are listed in Table S1 of the Supporting Information. The expression of IL1β, IL6, TNFα, IL10, and TGFβ1 inflammatory genes was determined using an SYBR Premix Ex Taq II kit (Takara Bio, USA).[45] The expression levels of the inflammatory genes were normalized with respect to β-actin, and the fold change was determined by the $\Delta\Delta Ct$ method.

Statistics. All values were expressed as the mean $\pm$ standard deviation. One-way and two-way ANOVA was carried out wherever applicable using GraphPadPrism (Version 6.01 software).

■ ASSOCIATED CONTENT

Supporting Information

The Supporting Information is available free of charge at https://pubs.acs.org/doi/10.1021/acsomega.0c01243.

FT-Raman spectra of ZM and ZMA (the band at 896 cm^{-1} indicates β-linkage); ^{1}H NMR spectra of ZMA in D_2O; particle size distribution native and aminated glucans in water; AFM images, particles of ZM, 3D view of ZM, particles of ZMA, and 3D view of ZMA; cytotoxicity of ZMA and ZM against Raw 264.7 cells; and list of primers used for the proinflammatory and anti-inflammatory study (PDF)

■ AUTHOR INFORMATION

Corresponding Author

Mukesh Doble − *Bioengineering and Drug Design Lab, Department of Biotechnology, IIT-Madras, Chennai 600036, India;* orcid.org/0000-0002-7533-3024; Phone: 91-44-2257-4107; Email: mukeshd@iitm.ac.in

Authors

Geetha Venkatachalam − *Bioengineering and Drug Design Lab, Department of Biotechnology, IIT-Madras, Chennai 600036, India*

Senthilkumar Arumugam − *Bioengineering and Drug Design Lab, Department of Biotechnology, IIT-Madras, Chennai 600036, India*

Complete contact information is available at: https://pubs.acs.org/10.1021/acsomega.0c01243

Notes

The authors declare no competing financial interest.

■ ACKNOWLEDGMENTS

G.V. thanks the Department of Science and Technology, Government of India, for financial support WOS-A (DST-SR/WOS-A/LS-391/2017). G.V. also thanks Dr. Nandakumar Venkatesan for helpful comments, English corrections, and suggestions. The authors thank the Sophisticated Analytical Instrument Facility (SAIF), IIT Madras, for analytical help.

■ ABBREVIATIONS

ZM,zymosan; ZMA,aminated zymosan; LPS,lipopolysaccharide; DAPI,(4′,6-diamidino-2-phenylindole); DMAE,dimethylaminoethyl; DMSO,dimethyl sulfoxide; $NaBH_4$,sodium borohydride; DMF,dimethylformamide; Ph_3P,triphenylphosphine; CBr_4,carbon tetrabromide or tetrabromomethane; MTT,3-(4,5-dimethylthiazol-2-yl)-2,5-diphenyltetrazolium bromide

■ REFERENCES

(1) Ohno, N.; Miura, T.; Miura, N. N.; Adachi, Y.; Yadomae, T. Structure and Biological Activities of Hypochlorite Oxidized Zymosan. *Carbohydr. Polym.* **2001**, *44*, 339−349.

(2) Ishimoto, Y.; Ishibashi, K.-I.; Yamanaka, D.; Adachi, Y.; Kanzaki, K.; Iwakura, Y.; Ohno, N. Production of Low-Molecular Weight Soluble Yeast β-Glucan by an Acid Degradation Method. *Int. J. Biol. Macromol.* **2018**, *107*, 2269−2278.

(3) Vetvicka, V.; Vetvickova, J. β- 1, 3-Glucan: Silver Bullet or Hot Air? *Open Glycosci.* **2010**, *3*, 1−6.

(4) Son, H. J.; Bae, H. C.; Kim, H. J.; Lee, D. H.; Han, D.-W.; Park, J.-C. Effects of β-Glucan on Proliferation and Migration of Fibroblasts. *Curr. Appl. Phys.* **2005**, *5*, 468−471.

(5) Wei, D.; Zhang, L.; Williams, D. L.; Browder, I. W. Glucan Stimulates Human Dermal Fibroblast Collagen Biosynthesis through a Nuclear Factor-1 Dependent Mechanism. *Wound Repair Regen.* **2002**, *10*, 161−168.

(6) Sato, M.; Sano, H.; Iwaki, D.; Kudo, K.; Konishi, M.; Takahashi, H.; Takahashi, T.; Imaizumi, H.; Asai, Y.; Kuroki, Y. Direct Binding of Toll-Like Receptor 2 to Zymosan, and Zymosan-Induced NF-KB Activation and TNF-α Secretion Are Down-Regulated by Lung Collectin Surfactant Protein A. *J. Immunol.* **2003**, *171*, 417.

(7) Utsunomiya, I.; Ito, M.; Oh-ishi, S. Generation of Inflammatory Cytokines in Zymosan-Induced Pleurisy in Rats: TNF Induces IL-6 and Cytokine-Induced Neutrophil Chemoattractant (CINC) in Vivo. *Cytokine* **1998**, *10*, 956−963.

(8) Takahashi, M.; Galligan, C.; Tessarollo, L.; Yoshimura, T. Monocyte Chemoattractant Protein-1 (MCP-1), Not MCP-3, Is the Primary Chemokine Required for Monocyte Recruitment in Mouse Peritonitis Induced with Thioglycollate or Zymosan A. *J. Immunol.* **2009**, *183*, 3463−3471.

(9) Conte, F. d. P.; Barja-Fidalgo, C.; Verri, W. A., Jr.; Cunha, F. Q.; Rae, G. A.; Penido, C.; Henriques, M. d. G. M. O. Endothelins Modulate Inflammatory Reaction in Zymosan-Induced Arthritis: Participation of LTB4, TNF-α, and CXCL-1. *J. Leukoc. Biol.* **2008**, *84*, 652−660.

(10) Friedland, J. S.; Constantin, D.; Shaw, T. C.; Stylianou, E. Regulation of Interleukin-8 Gene Expression after Phagocytosis of Zymosan by Human Monocytic Cells. *J. Leukoc. Biol.* **2001**, *70*, 447−454.

(11) Kolaczkowska, E.; Chadzinska, M.; Scislowska-Czarnecka, A.; Plytycz, B.; Opdenakker, G.; Arnold, B. Gelatinase B/Matrix Metalloproteinase-9 Contributes to Cellular Infiltration in a Murine Model of Zymosan Peritonitis. *Immunobiology* **2006**, *211*, 137−148.

(12) Di Carlo, F. J.; Fiore, J. V. On the Composition of Zymosan. *Science* **1958**, *127*, 756−757.

(13) Xia, Y.; Vetvicka, V.; Yan, J.; Hanikýrová, M.; Mayadas, T.; Ross, G. D. The β-Glucan-Binding Lectin Site of Mouse CR3 (CD11b/CD18) and Its Function in Generating a Primed State of the Receptor That Mediates Cytotoxic Activation in Response to IC3b-Opsonized Target Cells. *J. Immunol.* **1999**, *162*, 2281−2290.

(14) Brown, G. D.; Taylor, P. R.; Reid, D. M.; Willment, J. A.; Williams, D. L.; Martinez-Pomares, L.; Wong, S. Y. C.; Gordon, S.

Dectin-1 Is a Major Beta-Glucan Receptor on Macrophages. *J. Exp. Med.* **2002**, *196*, 407−412.
(15) Zimmerman, J. W.; Lindermuth, J.; Fish, P. A.; Palace, G. P.; Stevenson, T. T.; DeMong, D. E. A Novel Carbohydrate-Glycosphingolipid Interaction between a Beta-(1-3)-Glucan Immunomodulator, PGG-Glucan, and Lactosylceramide of Human Leukocytes. *J. Biol. Chem.* **1998**, *273*, 22014−22020.
(16) Rice, P. J.; Kelley, J. L.; Kogan, G.; Ensley, H. E.; Kalbfleisch, J. H.; Browder, I. W.; Williams, D. L. Human Monocyte Scavenger Receptors Are Pattern Recognition Receptors for (1→3)-*β*-D-Glucans. *J. Leukoc. Biol.* **2002**, *72*, 140−146.
(17) Teng, H.; Chen, L. *α*-Glucosidase and *α*-Amylase Inhibitors from Seed Oil: A Review of Liposoluble Substance to Treat Diabetes. *Crit. Rev. Food Sci. Nutr.* **2017**, *57*, 3438−3448.
(18) Chen, L.; Teng, H.; Xie, Z.; Cao, H.; Cheang, W. S.; Skalicka-Woniak, K.; Georgiev, M. I.; Xiao, J. Modifications of Dietary Flavonoids towards Improved Bioactivity: An Update on Structure-Activity Relationship. *Crit. Rev. Food Sci. Nutr.* **2018**, *58*, 513−527.
(19) Teng, H.; Chen, L. Polyphenols and Bioavailability: An Update. *Crit. Rev. Food Sci. Nutr.* **2019**, *59*, 2040−2051.
(20) Chen, L.; Teng, H.; Cao, H. Chlorogenic Acid and Caffeic Acid from Sonchus Oleraceus Linn Synergistically Attenuate Insulin Resistance and Modulate Glucose Uptake in HepG2 Cells. *Food Chem. Toxicol.* **2019**, *127*, 182−187.
(21) Salgado, M.; Rodríguez-Rojo, S.; Reis, R. L.; Cocero, M. J.; Duarte, A. R. C. Preparation of Barley and Yeast *β*-Glucan Scaffolds by Hydrogel Foaming: Evaluation of Dexamethasone Release. *J. Supercrit. Fluids* **2017**, *127*, 158−165.
(22) Gao, Y.; Jiang, R.; Qie, J.; Chen, Y.; Xu, D.; Liu, W.; Gao, Q. Studies on the Characteristic and Activity of Low-Molecular Fragments from Zymosan. *Carbohydr. Polym.* **2012**, *90*, 1411−1414.
(23) Hida, S.; Nagi-Miura, N.; Adachi, Y.; Ohno, N. Beta-Glucan Derived from Zymosan Acts as an Adjuvant for Collagen-Induced Arthritis. *Microbiol. Immunol.* **2006**, *50*, 453−461.
(24) Hwang, J.; Lee, K.; Gilad, A. A.; Choi, J. Synthesis of Beta-Glucan Nanoparticles for the Delivery of Single Strand DNA. *Biotechnol. Bioprocess Eng.* **2018**, *23*, 144−149.
(25) Yiannikouris, A.; François, J.; Poughon, L.; Dussap, C.-G.; Bertin, G.; Jeminet, G.; Jouany, J.-P. Alkali Extraction of *β*-d-Glucans from Saccharomyces Cerevisiae Cell Wall and Study of Their Adsorptive Properties toward Zearalenone. *J. Agric. Food Chem.* **2004**, *52*, 3666−3673.
(26) Han, J.; Cai, J.; Borjihan, W.; Ganbold, T.; Rana, T. M.; Baigude, H. Preparation of Novel Curdlan Nanoparticles for Intracellular SiRNA Delivery. *Carbohydr. Polym.* **2015**, *117*, 324−330.
(27) Borjihan, G.; Zhong, G.; Baigude, H.; Nakashima, H.; Uryu, T. Synthesis and Anti-HIV Activity of 6-Amino-6-Deoxy-(1→3 -*β*-D-Curdlan Sulfate. *Polym. Adv. Technol.* **2003**, *14*, 326−329.
(28) Ishimoto, Y.; Ishibashi, K.-I.; Yamanaka, D.; Adachi, Y.; Kanzaki, K.; Okita, K.; Iwakura, Y.; Ohno, N. Modulation of an Innate Immune Response by Soluble Yeast Beta-Glucan Prepared by a Heat Degradation Method. *Int. J. Biol. Macromol.* **2017**, *104*, 367−376.
(29) Shin, M. S.; Lee, S.; Lee, K. Y.; Lee, H. G. Structural and Biological Characterization of Aminated-Derivatized Oat Beta-Glucan. *J. Agric. Food Chem.* **2005**, *53*, 5554−5558.
(30) Lee, J. Structural Modification of Polysaccharide for the Improvement of Functionality. Ph. D. Thesis, Korea Advanced Institute of Science and Technology, 1998.
(31) Wang, L. C.; Zhang, K.; Di, L. Q.; Liu, R.; Wu, H. Isolation and Structural Elucidation of Novel Homogenous Polysaccharide from Mactra Veneriformis. *Carbohydr. Polym.* **2011**, *86*, 982−987.
(32) Wang, H.-x.; Zhao, J.; Li, D.-m.; Song, S.; Song, L.; Fu, Y.-h.; Zhang, L.-p. Structural Investigation of a Uronic Acid-Containing Polysaccharide from Abalone by Graded Acid Hydrolysis Followed by PMP-HPLC−MSn and NMR Analysis. *Carbohydr. Res.* **2015**, *402*, 95−101.
(33) Saito, H.; Ohki, T.; Sasaki, T. A 13C Nuclear Magnetic Resonance Study of Gel-Forming (1 Goes to 3)-Beta-d-Glucans. Evidence of the Presence of Single-Helical Conformation in a Resilient Gel of a Curdlan-Type Polysaccharide 13140 from Alcaligenes Faecalis Var. Myxogenes IFO 13140. *Biochemistry* **1977**, *16*, 908−914.
(34) Wang, L.; Chen, L.; Li, J.; Di, L.; Wu, H. Structural Elucidation and Immune-Enhancing Activity of Peculiar Polysaccharides Fractioned from Marine Clam Meretrix Meretrix (Linnaeus). *Carbohydr. Polym.* **2018**, *201*, 500−513.
(35) Cruz, A. K. M.; Andrade, G. P. V.; Chavante, S. F.; de Vasconcelos, C. L.; Leite, E. L.; Valente, A. P.; Sales, M. P.; Oliveira, F. W.; Oliveira, F. W. Structural Elucidation of an Acidic Galactan from the Eggs of Mollusc Pomacea Lineata. *Carbohydr. Polym.* **2010**, *79*, 975−980.
(36) Lee, S.; Seo, D.-H.; Park, H.-L.; Choi, Y.; Jung, S. Solubility Enhancement of a Hydrophobic Flavonoid, Luteolin by the Complexation with Cyclosophoraoses Isolated from Rhizobium Meliloti. *Antonie Leeuwenhoek* **2003**, *84*, 201−207.
(37) Venkatachalam, G.; Nandakumar, V.; Suresh, G.; Doble, M. Characterization and applications of cyclic *β*-(1,2)-glucan produced from R. meliloti. *RSC Adv.* **2014**, *4*, 11393−11399.
(38) Kawaharada, Y.; Kiyota, H.; Eda, S.; Minamisawa, K.; Mitsui, H. Structural Characterization of Neutral and Anionic Glucans from Mesorhizobium Loti. *Carbohydr. Res.* **2008**, *343*, 2422−2427.
(39) Muschin, T.; Yoshida, T. Structural Analysis of Galactomannans by NMR Spectroscopy. *Carbohydr. Polym.* **2012**, *87*, 1893−1898.
(40) Hernanz-Falcón, P.; Joffre, O.; Williams, D. L.; Reis e Sousa, C. Internalization of Dectin-1 Terminates Induction of Inflammatory Responses. *Eur. J. Immunol.* **2009**, *39*, 507−513.
(41) Ren, T.; Gou, J.; Sun, W.; Tao, X.; Tan, X.; Wang, P.; Zhang, Y.; He, H.; Yin, T.; Tang, X. Entrapping of Nanoparticles in Yeast Cell Wall Microparticles for Macrophage-Targeted Oral Delivery of Cabazitaxel. *Mol. Pharm.* **2018**, *15*, 2870−2882.
(42) Novák, M.; Synytsya, A.; Gedeon, O.; Slepička, P.; Procházka, V.; Synytsya, A.; Blahovec, J.; Hejlová, A.; Čopíková, J. Yeast *β*(1-3), (1-6)-d-Glucan Films: Preparation and Characterization of Some Structural and Physical Properties. *Carbohydr. Polym.* **2012**, *87*, 2496−2504.
(43) Hunter, K. W.; Gault, R. A.; Berner, M. D. Preparation of Microparticulate Beta-Glucan from Saccharomyces Cerevisiae for Use in Immune Potentiation. *Lett. Appl. Microbiol.* **2002**, *35*, 267−271.
(44) López-García, J.; Lehocký, M.; Humpolíček, P.; Sáha, P. HaCaT Keratinocytes Response on Antimicrobial Atelocollagen Substrates: Extent of Cytotoxicity, Cell Viability and Proliferation. *J. Funct. Biomater.* **2014**, *5*, 43−57.
(45) Yunus Basha, R.; Sampath, S. K.; Doble, M. Dual Delivery of Tuberculosis Drugs via Cyclodextrin Conjugated Curdlan Nanoparticles to Infected Macrophages. *Carbohydr. Polym.* **2019**, *218*, 53−62.
(46) Yunus Basha, R.; Sampath Kumar, T. S.; Selvaraj, R.; Doble, M. Silver Loaded Nanofibrous Curdlan Mat for Diabetic Wound Healing: An In Vitro and In Vivo Study. *Macromol. Mater. Eng.* **2018**, *303*, 1800234.
(47) Li, Y.-Z.; Chen, J.-H.; Tsai, C.-F.; Yeh, W.-L. Anti-Inflammatory Property of Imperatorin on Alveolar Macrophages and Inflammatory Lung Injury. *J. Nat. Prod.* **2019**, *82*, 1002−1008.
(48) Tesz, G. J.; Aouadi, M.; Prot, M.; Nicoloro, S. M.; Boutet, E.; Amano, S. U.; Goller, A.; Wang, M.; Guo, C.-A.; Salomon, W. E.; Virbasius, J. V.; Baum, R. A.; O'Connor, M. J.; Soto, E.; Ostroff, G. R.; Czech, M. P. Glucan Particles for Selective Delivery of SiRNA to Phagocytic Cells in Mice. *Biochem. J.* **2011**, *436*, 351−362.
(49) Goodridge, H. S.; Wolf, A. J.; Underhill, D. M. Beta-Glucan Recognition by the Innate Immune System. *Immunol. Rev.* **2009**, *230*, 38−50.
(50) Kerrigan, A. M.; Brown, G. D. Syk-Coupled C-Type Lectin Receptors That Mediate Cellular Activation via Single Tyrosine Based Activation Motifs. *Immunol. Rev.* **2010**, *234*, 335−352.
(51) Kuhn, D. A.; Vanhecke, D.; Michen, B.; Blank, F.; Gehr, P.; Petri-Fink, A.; Rothen-Rutishauser, B. Different Endocytotic Uptake

Mechanisms for Nanoparticles in Epithelial Cells and Macrophages. *Beilstein J. Nanotechnol.* **2014**, *5*, 1625−1636.
(52) Zhang, B.; Feng, X.; Yin, H.; Ge, Z.; Wang, Y.; Chu, Z.; Raabova, H.; Vavra, J.; Cigler, P.; Liu, R.; Wang, Y.; Li, Q. Anchored but Not Internalized: Shape Dependent Endocytosis of Nanodiamond. *Sci. Rep.* **2017**, *7*, 46462.
(53) Li, D.-Q.; Zhou, N.; Zhang, L.; Ma, P.; Pflugfelder, S. C. Suppressive Effects of Azithromycin on Zymosan-Induced Production of Proinflammatory Mediators by Human Corneal Epithelial Cells. *Invest. Ophthalmol. Vis. Sci.* **2010**, *51*, 5623−5629.
(54) Marinelli, C.; Di Liddo, R.; Facci, L.; Bertalot, T.; Conconi, M. T.; Zusso, M.; Skaper, S. D.; Giusti, P. Ligand Engagement of Toll-like Receptors Regulates Their Expression in Cortical Microglia and Astrocytes. *J. Neuroinflammation* **2015**, *12*, 244.
(55) Borjihan, G.; Zhong, G.; Baigude, H.; Nakashima, H.; Uryu, T. Synthesis and Anti-HIV Activity of -6-Amino-6-Deoxy-(1→3)-β-D-Curdlan Sulfate. *Polym. Adv. Technol.* **2003**, *14*, 326−329.
(56) Aparnadevi, N.; Saravana Kumar, K.; Manikandan, M.; Paul Joseph, D.; Venkateswaran, C. Room Temperature Dual Ferroic Behaviour of Ball Mill Synthesized NdFeO3 Orthoferrite. *J. Appl. Phys.* **2016**, *120*, 034101.
(57) Venkatachelam, G.; Divyaa Srinivasan, M. D. Cyclic β-(1, 2)-Glucan Production by Rhizobium Meliloti MTCC 3402. *Process Biochem.* **2013**, *48*, 1848−1854.
(58) Xu, W.; Pan, R.; Zhao, D.; Chu, D.; Wu, Y.; Wang, R.; Chen, B.; Ding, Y.; Sadatmousavi, P.; Yuan, Y.; Chen, P. Design and Evaluation of Endosomolytic Biocompatible Peptides as Carriers for SiRNA Delivery. *Mol. Pharm.* **2015**, *12*, 56−65.
(59) Prabhakar, P. K.; Raj, S.; Anuradha, P. R.; Sawant, S. N.; Doble, M. Biocompatibility Studies on Polyaniline and Polyaniline-Silver Nanoparticle Coated Polyurethane Composite. *Colloids Surf. B Biointerfaces* **2011**, *86*, 146−153.
(60) Hajiali, H.; Summa, M.; Russo, D.; Armirotti, A.; Brunetti, V.; Bertorelli, R.; Athanassiou, A.; Mele, E. Alginate−Lavender Nanofibers with Antibacterial and Anti-Inflammatory Activity to Effectively Promote Burn Healing. *J. Mater. Chem. B* **2016**, *4*, 1686−1695.

https://dx.doi.org/10.1021/acsomega.0c01243
ACS Omega 2020, 5, 15973−15982